NANO LETTERS

pubs.acs.org/NanoLett
Letter

Strong Coupling of Coherent Phonons to Excitons in Semiconducting Monolayer $MoTe_2$

Charles J. Sayers, Armando Genco, Chiara Trovatello, Stefano Dal Conte, Vladislav O. Khaustov, Jorge Cervantes-Villanueva, Davide Sangalli, Alejandro Molina-Sanchez, Camilla Coletti, Christoph Gadermaier, and Giulio Cerullo*

Cite This: *Nano Lett.* 2023, 23, 9235−9242

ABSTRACT: The coupling of the electron system to lattice vibrations and their time-dependent control and detection provide unique insight into the nonequilibrium physics of semiconductors. Here, we investigate the ultrafast transient response of semiconducting monolayer 2*H*-$MoTe_2$ encapsulated with *h*BN using broadband optical pump−probe microscopy. The sub-40 fs pump pulse triggers extremely intense and long-lived coherent oscillations in the spectral region of the A′ and B′ exciton resonances, up to ∼20% of the maximum transient signal, due to the displacive excitation of the out-of-plane A_{1g} phonon. Ab initio calculations reveal a dramatic rearrangement of the optical absorption of monolayer $MoTe_2$ induced by an out-of-plane stretching and compression of the crystal lattice, consistent with an A_{1g} -type oscillation. Our results highlight the extreme sensitivity of the optical properties of monolayer TMDs to small structural modifications and their manipulation with light.

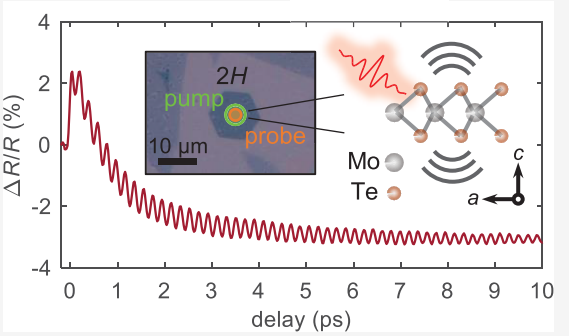

KEYWORDS: *Coherent phonons, excitons, ultrafast spectroscopy, transition metal dichalcogenides, two-dimensional materials, monolayer, $MoTe_2$*

Electron−phonon coupling is crucially important to many phenomena in condensed matter, such as carrier scattering in transport,[1−3] the relaxation of photoinduced nonequilibrium quasiparticle populations,[4−10] and electronic order emerging at low temperatures.[11−14] Photoexcitation of coherent phonons (CPs) using ultrashort light pulses enables fundamental insight into electron−phonon interactions via their excitation and detection mechanisms,[15−17] which has led to discoveries such as elucidating the role of vibrational coherence in the primary event of vision,[18] detecting coherent Bloch oscillations in coupled semiconductor quantum wells,[19] and demonstrating THz radiation emission due to the macroscopic polarization originating from CPs.[20] There is potential for applications in sensors, actuators, and transducers[21−24] operating at frequencies up to several THz.[25] In semiconductors with large exciton binding energies, photoexcitation of CPs has provided vital information about exciton−phonon coupling.[26−29]

Two-dimensional semiconductors such as monolayer transition-metal dichalcogenides (TMDs) combine strong light-matter interaction and multifaceted exciton and valley physics with a great potential for applications in energy harvesting and information processing.[30−35] An important tool in the investigation of exciton-coherent phonon coupling in these materials is femtosecond transient absorption (TA) spectroscopy. Here, an initial ultrashort pump pulse photoexcites the sample, while a second delayed probe pulse is used to measure the transient change in the optical response. This allows for tracking the temporal evolution of the nonequilibrium quasiparticle populations, which manifests as the characteristic decay time of the TA signal. In WSe_2, it has previously been shown that coherent oscillations of the out-of-plane A_{1g} phonon mode introduce a small modulation (∼10^{-3} of the transient signal) on the electronic relaxation at the optical bandgap.[36] Similarly, in monolayer MoS_2, the oscillatory modulation of the TA signal has also been ascribed to CPs belonging to the A_{1g} mode, which exhibit a relatively small amplitude across the spectral region of the A and B exciton resonances,[36] but a significant modulation of ∼2% of the maximum signal around the C exciton.[28]

$MoTe_2$ is a TMD with two well-known thermodynamically stable polymorphs with distinct electronic properties. Its

Received: May 24, 2023
Revised: September 19, 2023
Published: September 26, 2023

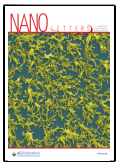

https://doi.org/10.1021/acs.nanolett.3c01936
Nano Lett. 2023, 23, 9235−9242

semimetallic phase,[37,38] (1T' above and T_d below 240 K) exhibits large magnetoresistance,[39] ferroelectricity,[40] and superconductivity.[41] The semiconducting 2H phase, on the other hand, has an indirect bandgap in the bulk which becomes direct (∼1.1 eV) toward the monolayer limit,[42,43] thus expanding the potential functionality of TMDs into the near-infrared (NIR). Furthermore, a high carrier mobility,[44] strong spin−orbit coupling,[45] valley selectivity,[46] and ambipolar transistor behavior,[47] make it a promising candidate for NIR optoelectronics, photovoltaics, and unconventional information encoding such as spintronics or valleytronics. However, since its lower chemical stability has been overcome only recently by encapsulation using few-layer hBN,[48] $MoTe_2$ is significantly less studied than its sulfur and selenium analogues. Previous TA experiments on 2H-$MoTe_2$ with various probe energies, ranging from 1.0 eV to 2.6 eV, have elucidated the dynamics of several excitonic transitions, but without detecting any CP signature thus far.[49−51] Optical pump-core level (XUV) probe spectroscopy, on the other hand, has revealed a strong oscillatory signal contribution dominated by the out-of-plane A_{1g} mode with a smaller E_{1g} component,[52] where the greatest oscillation amplitude was observed for transitions from the Te-4$d_{5/2}$ levels to the conduction band.

Here, we employ broadband TA microscopy to study the coupling of the out-of-plane A_{1g} vibrational mode in semiconducting monolayer 2H-$MoTe_2$ to several excitonic resonances. Our work is supported by ab initio simulations, which combine density functional and perturbation theory (DFT/DFPT) with many-body perturbation theory (GW+BSE). We find an exceptionally strong and long-lived oscillatory signal contribution, which is rarely observed in semiconducting TMDs. Our broadband probe combined with an excellent temporal resolution of ≲40 fs reveals the spectral dependence of the amplitude and phase of CPs with exceptional clarity. Our simulations confirm a strong modulation of the electronic band structure and, consequently, the absorption spectrum by out-of-plane atomic motion, allowing the theoretical prediction of the spectral profile of the oscillation amplitude in excellent agreement with the experimental observations. Our results demonstrate how the optical properties of monolayer $MoTe_2$ in the visible and NIR range are highly susceptible to manipulation via small structural modifications and how these can be controlled optically using ultrashort light pulses.

Samples of $MoTe_2$ were synthesized by chemical vapor deposition on Si/SiO_2 and encapsulated with few-layer hBN according to the methods in ref 48. The procedure yields flakes of both polymorphs, which are easily distinguished by their shape; elongated for 1T', or hexagonal for 2H. Since the 2H flakes have a lateral size of only a few micrometers, we employed a broadband optical pump−probe microscope[53] whereby pump and probe are focused onto the sample using an objective lens, as illustrated in Figure 1a, providing a spatial resolution of ∼3 μm. The Raman spectrum measured on the same flake, shown in Figure 1b, confirms the semiconducting 2H polymorph, with the most prominent peak at 235 cm^{-1} originating from the in-plane E_{2g} phonon. A further peak, seen here at 170 cm^{-1}, is associated with the out-of-plane A_{1g} phonon and has been shown in previous studies to be clearly visible for excitation at 633 nm (1.96 eV), but much weaker for excitation at 532 nm (2.33 eV).[42] The absence of modes at 120 and 290 cm^{-1} confirms the flake to be monolayer.[42,54] The calculated absorption spectrum of monolayer 2H-$MoTe_2$,

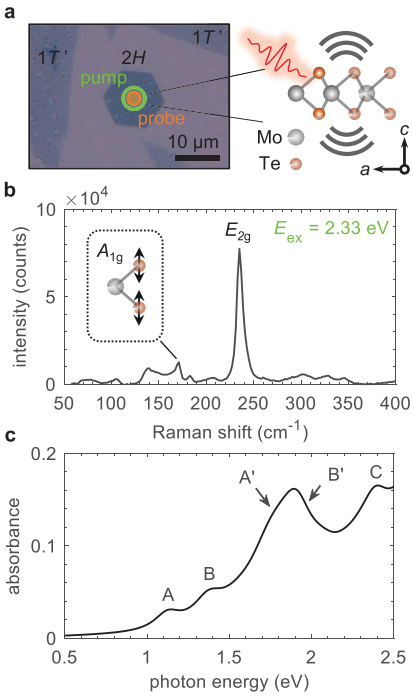

Figure 1. Optical properties of monolayer 2H-$MoTe_2$. (a) Microscope image of hBN encapsulated monolayer $MoTe_2$ samples on Si/SiO_2 (left). Optical pump−probe microscopy experiments were performed on the 2H region with pump (∼5 μm) and probe (∼3 μm) beam diameters, as illustrated. The optical pulse launches an intense out-of-plane (c-axis) vibration of the lattice (right). (b) Raman spectrum of the $MoTe_2$ sample measured with 532 nm (∼2.33 eV) excitation. The out-of-plane vibration with A_{1g} symmetry is highlighted. (c) Optical absorption spectrum for the equilibrium structure from ab initio calculations. Optical transitions are labeled according to the convention of ref 55.

shown in Figure 1c, exhibits a series of excitonic resonances, whose energies and relative intensities match closely with previously measured spectra.[42,55]

We now investigate the transient dynamics of monolayer $MoTe_2$ at T = 10 K after photoexcitation with a pump centered at ∼2.36 eV. We measure the differential reflectance, $\Delta R/R$ with a broadband probe in the range ∼1.7−2.6 eV at variable delay after excitation. The pump and probe beams are focused and spatially overlapped on the sample, as indicated in Figure 1a. The probe is detected in backscattering geometry after interaction with the hBN-$MoTe_2$−Si/SiO_2 sample stack. The dominant effect of photoexcitation is a change in the absorption spectrum of the $MoTe_2$ layer, and, hence, we assume the measured differential reflectance, $\Delta R/R$ to be proportional to ΔA, i.e., the change in absorbance of $MoTe_2$. Further details are provided in the Methods section of the Supporting Information.

The transient $\Delta R/R$ spectra, shown over the first 5 ps in Figure 2a, exhibit two positive bands of increased reflectivity upon photoexcitation and two negative bands of decreased reflectivity. The positive $\Delta R/R$ signal is ascribed to the photobleaching (PB) of the excitonic transitions. The PB peaks from 1.75 eV to 2.2 eV and above 2.4 eV match the positions of the A′, B′, and C excitonic resonances according to ref 42 (see also Figure 2b), suggesting a reduced absorption due to Pauli blocking. The negative $\Delta R/R$ signal instead originates from exciton energy renormalization, which causes a shift of

https://doi.org/10.1021/acs.nanolett.3c01936
Nano Lett. 2023, 23, 9235−9242

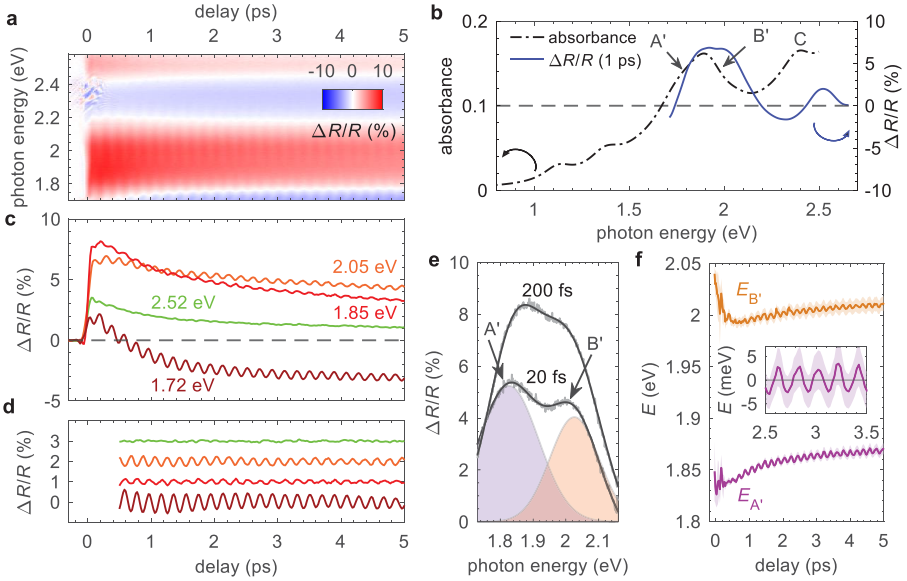

Figure 2. Transient optical response of monolayer 2*H*-$MoTe_2$. (a) Broadband differential reflectance ($\Delta R/R$) maps following excitation with a pump photon energy of 2.36 eV and a fluence of 500 μJ cm^{-2}. The sample temperature was 10 K. (b) Transient $\Delta R/R$ spectrum (right axis) at 1 ps delay compared to the calculated optical absorbance of the equilibrium structure (left axis). (c) Dynamics extracted at various probe photon energies, as indicated. (d) Isolated coherent component of the $\Delta R/R$ signal after subtraction of a biexponential fit to the incoherent dynamics in panel (c). Data are offset for clarity. (e) $\Delta R/R$ spectra at early times (20 and 200 fs) showing two positive peaks related to the A′ and B′ transitions. The bold solid lines are fits to the data using a multiple Gaussian procedure, where the shaded areas show the two individual components for the A′ (purple) and B′ (orange) peaks. (f) Temporal evolution of the peak center energies, $E_{A'}$ and $E_{B'}$ obtained from the fitting in panel (e). The inset shows the energy modulation of the $E_{A'}$ peak after subtraction of a biexponential. The shaded areas are the associated fitting errors.

the transition and induces a change of sign in the pump−probe signal, from 2.2 eV to 2.4 eV and below 1.75 eV.[56,57] Immediately after photoexcitation, an increase of the electronic temperature broadens the exciton line shape, which subsequently narrows at longer delay times. The extracted exciton dynamics are shown in Figure 2c. After a nearly instantaneous rise time, i.e., limited by the temporal resolution of the experiment, the PB signal related to the A′ and B′ resonances decays with time constants of the order τ_{fast} = 0.7−0.8 ps and τ_{slow} = 6.0−8.0 ps (see Figure S1 in the Supporting Information), without further significant changes of spectral shape.

We now turn our attention to the oscillations, clearly visible in the spectral region from 1.7 eV to 2.3 eV (see Figures 2a and 2c), which we assign to photoexcited CPs.[28] Such oscillations have not been observed in previous work on $MoTe_2$ for a probe in the visible range.[49−51] Here, however, we find an exceptionally strong coherent (oscillatory) component with a magnitude of up to 20% of the maximum $\Delta R/R$ signal, which is an order of magnitude greater than the CP amplitude (2%) found in monolayer MoS_2.[28] The isolated oscillatory component, shown in Figure 2d, obtained by subtracting the incoherent (nonoscillatory) signal contribution with a biexponential decay, can be fitted with a single damped cosine term (see Figure S2 in the Supporting Information). The CP mode, measured at 10 K, has a period of 194 fs, which corresponds to a frequency of 5.15 THz (~172 cm^{-1}), and an energy of 21 meV. The A_{1g} Raman mode frequency in Figure 1b, measured instead at 295 K, is 5.10 THz (~170 cm^{-1}), consistent with our observations of the CP mode at 295 K (see Figure S3 in the Supporting Information) and the expected temperature-induced mode softening. Therefore, based on this agreement, and previous observations in pump−probe studies of TMDs,[14,28] we assign the CP mode to the out-of-plane A_{1g} vibration. The CP component lasts for tens of picoseconds and exhibits a damping time of τ_{damp} = (6.25 ± 0.25) ps, suggesting that vibrational dephasing is weak. Interestingly, we find that the phonon lifetime is almost independent of temperature between 10 K and 295 K (see Figure S3), which has also been noted in Raman spectroscopy studies,[58] implying an extremely weak phonon decay, for example, via phonon−phonon scattering, consistent with both the long-lived CP signal observed here and its negligible anharmonicity (constant frequency over 10 ps). Finally, by performing a Gaussian fitting procedure for the positive PB signal corresponding to the A′ and B′ contributions, as shown in Figure 2e, we can obtain the temporal dynamics of the peak energies (Figure 2f). Both PB peaks are initially red-shifted by the photoexcitation and follow similar recovery dynamics. We find that the peak energies of both A′ and B′ resonances are also modulated (with matching phase) by the A_{1g} vibration with an amplitude of ~2.5 meV or 5 meV peak-to-peak, as highlighted in the inset of Figure 2f.

For the excitation mechanism of CPs, two main processes are customarily invoked: impulsive stimulated Raman scattering (ISRS),[59] and displacive excitation of coherent phonons (DECP).[60] In ISRS, the CPs have a pump energy dependence that follows the excitation profile of the Raman tensor. The pump pulse transmits kinetic energy to the lattice atoms during a time interval much shorter than the oscillation period. At t = 0, the atoms are in a quasi-equilibrium position, resulting in a sine oscillation. In DECP, on the other hand, the population of excited states changes the potential energy surface and thus the quasi-equilibrium position of the lattice. Therefore, at t = 0, the lattice is at a maximum or minimum of the oscillating nuclear coordinate, resulting in cosine oscillation. The high time resolution of our experiment allows a precise determination of the phase of the oscillatory $\Delta R/R$ component and the identification of the cosine oscillation characteristic of DECP

https://doi.org/10.1021/acs.nanolett.3c01936
Nano Lett. 2023, 23, 9235−9242

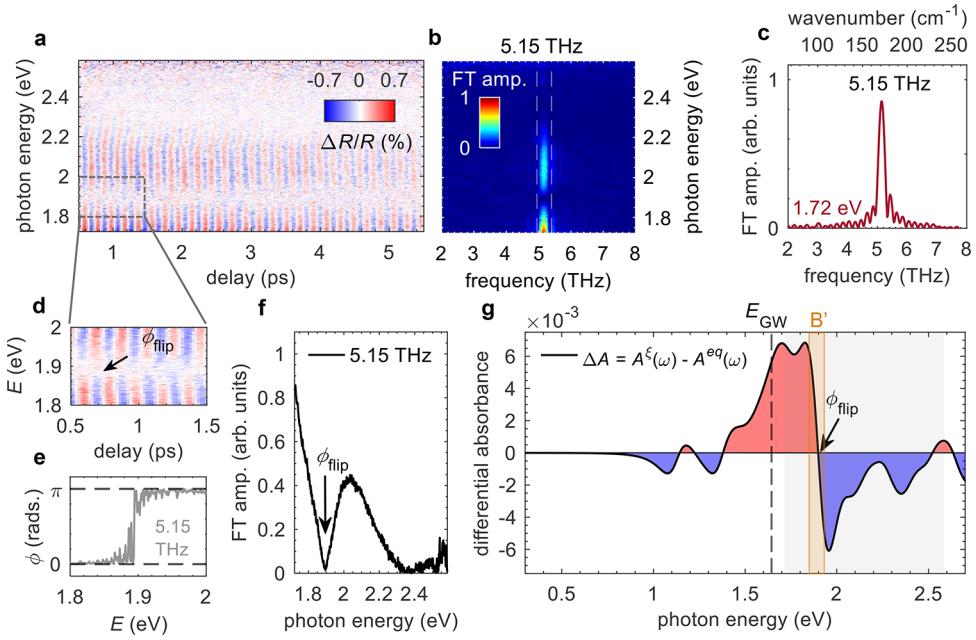

Figure 3. Frequency analysis of coherent phonon oscillations in monolayer 2*H*-$MoTe_2$. (a) Coherent component of the transient signal map, $\Delta R/R$. (b) Fourier transform (FT) map of the data in panel a. (c) FT frequency spectrum extracted at 1.72 eV, showing a peak at ∼5.15 THz (∼172 cm^{-1}). (d) Coherent component map showing the energy range 1.8−2.0 eV near to the phase flip, labeled ϕ_{flip}. (e) FT phase spectrum confirming the phase flip from 0 to π, which occurs at ∼1.89 eV. (f) FT amplitude spectrum extracted at 5.15 THz (vertical dashed area in panel (b)). (g) Differential absorbance spectrum, $A^{\xi}(\omega) - A^{eq}(\omega)$ from ab initio calculations. The vertical dashed line indicates the GW direct bandgap energy, while the orange shaded area shows the B′ exciton transition. The gray shaded area highlights the experimentally explored energy range.

(see Figure S4 in the Supporting Information). Moreover, we find that the oscillations in $MoTe_2$ have similar magnitudes, or are slightly enhanced, for excitation at 2.36 eV, compared to 1.91 eV (see Figure S5 in the Supporting Information), while the Raman peak at 170 cm^{-1} is much weaker for excitation energy at 2.33 eV, corroborating the identification of different excitation mechanisms for Raman scattering and CPs.

The spectral window where CP modulation of $\Delta R/R$ is visible, as seen in Figures 3a and 3b, can be divided into two regions: above and below 1.89 eV, where the oscillations have opposite sign equivalent to a phase difference of π. The Fourier transform of the CP in Figures 3b and 3c shows a single prominent mode with a constant frequency of 5.15 THz over the entire probe window. Its amplitude, however, as shown in Figure 3f, changes dramatically over the range of 1.7−2.3 eV, with a maximum at or below the lowest probe energy (1.72 eV), and a zero at ∼1.89 eV associated with a π-phase flip occurring at this energy, which is directly visible in the data in Figure 3d, and confirmed by Fourier analysis in Figure 3e.

To gain further insight into the probe energy dependence of the amplitude and phase of the 5.15 THz vibration, we calculated the change in the absorption spectrum caused by out-of-plane displacement of the Te atoms around the central Mo along the *c*-axis, mimicking an A_{1g} -type oscillation launched by the pulse. Starting from the result of the BSE calculations, as described in the Methods section of the Supporting Information, we obtain the polarizability per unit area, $\alpha_{2D}(\omega)$, and define an effective dielectric tensor, $\epsilon_{2D}(\omega)$ which takes into account the effects of quantum confinement in two dimensions:[61]

$$\epsilon_{2D}(\omega) = 1 + \frac{4\pi\alpha_{2D}(\omega)}{\Delta z}$$

where Δz is the material thickness. In the case of monolayer $MoTe_2$, the theoretical value is Δz = 7.66 Å. The dielectric tensor is used to compute the absorbance, according to the expression[62]

$$A(\omega) = \frac{\omega}{c}\mathrm{Im}[\epsilon_{2D}](\omega)\Delta z$$

The differential absorbance, ΔA was then calculated by subtracting the absorbance of the equilibrium structure, A^{eq} from the absorbance, $A^{\xi}(\alpha)$ with atoms displaced by a fixed amount, α along the A_{1g} phonon mode, ξ. The differential absorbance measured experimentally is small enough to be described in terms of a linear dependence on the atomic displacement α, i.e., $A^{\xi}(\alpha) \simeq A^{eq} + \partial_{\alpha}A^{\xi}\alpha$. In the numerical simulations, α was fixed to obtain a stretching along the *c*-axis equivalent to 0.5% of the Mo−Te bond length, measured from the center of the atoms.

The result, shown in Figure 3g, reproduces both the Fourier spectrum and the phase flip remarkably across the experimental energy window (gray-shaded area). The calculated spectrum reveals a rich structure consisting of multiple optical transitions, where the peak widths have been inferred. Most notably, the spectrum is dominated by a large contribution centered at ∼2 eV, which corresponds to the B′ exciton absorption, suggesting a particularly strong coupling of this transition with the A_{1g} mode. The theoretical phase flip energy was found to be 1.90 eV, in almost perfect agreement with that observed experimentally.

We now inspect the effects of the A_{1g} mode atomic displacement on the electronic and optical properties of $MoTe_2$ in more detail. Figure 4a shows calculations of the optical absorption of a monolayer in equilibrium, including excitonic effects, compared to stretching (red line) and compression (blue line) of 0.5% along the *c*-axis. The main

https://doi.org/10.1021/acs.nanolett.3c01936
Nano Lett. 2023, 23, 9235−9242

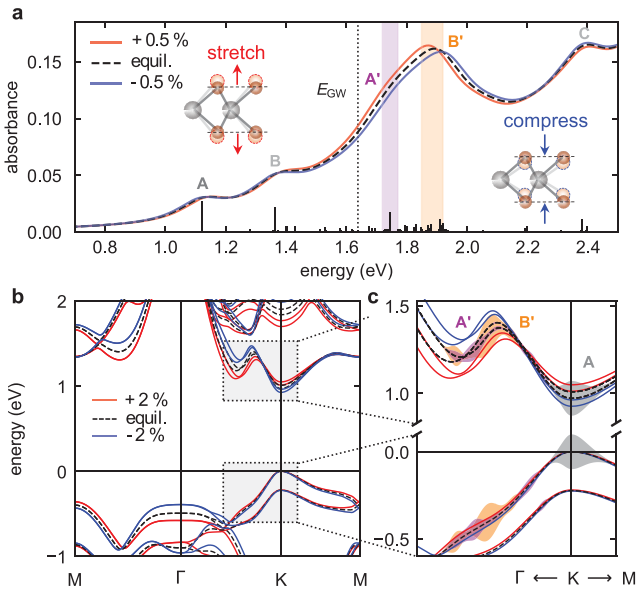

Figure 4. Optical and electronic properties of monolayer 2*H*-$MoTe_2$ from ab initio calculations. (a) Optical absorption spectra for vertical stretching (red) and compression (blue) along the *c*-axis direction of the Mo−Te bond length equivalent to 0.5%. The spectrum of the equilibrium structure (dashed line), i.e., no stretching or compression, is shown for comparison. The purple- and orange-shaded areas indicate the A' and B' exciton resonances, respectively. The dashed vertical line is the GW direct bandgap energy, E_{GW}. The black vertical bars correspond to the poles of the excitonic matrix, where their height is proportional to the oscillator strength. (b) Electronic band structure for 2% stretching (red) and compression (blue). (c) Selected region around the *K*-point. The shaded areas represent the energy-momentum distribution of the optical transitions related to the A, A′, and B′ excitons for the equilibrium structure, as indicated.

features (labeled in Figure 4a) are reproduced with excellent agreement to previous works[42,55] starting from the lowest energy A exciton at ∼1.1 eV. In particular, we emphasize the position of the B′ transition at ∼2 eV, which is located within the continuum beyond the GW direct bandgap, and, hence, a large number of transitions (orange-shaded area) have been taken into account to analyze it correctly. The optical absorption is subtly different except for the spectral region of 1.6−2.1 eV, where there is dramatic rearrangement in both energy and magnitude. For out-of-plane compression, the A′ and B′ resonances shift to higher energies, with the B′ peak shifting more significantly, which leads to a larger separation of the two overlapping peaks, while upon stretching they shift to lower energies, increasing the overlap and forming a single, more intense peak. Consistently with our experimental results, the strongest modulation of the absorption occurs on the low energy side of the double peak with a relative change of ∼10% for 0.5% out-of-plane displacement.

The particularly strong coupling of the B′ exciton with the A_{1g} mode leads to an energy shift of the absorption around the equilibrium position as the atoms oscillate. Such an energy modulation was observed in the experiments (Figure 2f), as discussed previously. In the displacive excitation of coherent phonons, photoexcitation changes the nuclear quasi-equilibrium positions, and at $t = 0$ the nuclei are displaced relative to this new quasi-equilibrium. Their oscillation results in a periodic modulation of the absorption spectrum. Following the oscillatory component at energies below 1.89 eV, we observe a positive $\Delta R/R$ at $t = 0$. Therefore, at $t = 0$ the spectrum is blue-shifted relative to its new quasi-equilibrium, meaning the out-of-plane positions of the Te atoms are at a minimum. Their new quasi-equilibrium position is at a larger distance than prior to photoexcitation. Above 1.89 eV the same blue shift results in an increase of the absorption and hence an oscillatory modulation of opposite sign, i.e., a phase shift of π.

To understand why the optical absorption exhibits such a dramatic change in a specific energy range, we now analyze the calculated electronic band structures, shown in Figures 4b and 4c, for a larger displacement of 2% in order to emphasize the effects. The calculations confirm the two valence band maxima and conduction band minima at the *K*-point, which give rise to the lowest energy excitonic transitions A and B, outside the spectral window of our experiment. The dominant change in the electronic structure at the *K*-point is bandgap renormalization, which results in a comparatively small energy shift of the A exciton transition. Instead, the A′ and B′ transitions, which appear as a broad double PB peak centered at ∼1.9 eV in the experiment, originate from regions of the band structure along the *K*−Γ direction, as illustrated by the shaded areas in Figure 4c. Here, we find that the atomic displacement results in considerable modification of the bands, especially close to the local minima and maxima of the conduction band, where optical transitions related to the A′ and B′ exciton are most important. The result is a large energy shift and change in the magnitude of the optical absorption in the spectral range close to these transitions, as shown in Figure 4a. We note that the A′ and B′ peaks in $MoTe_2$ are much narrower in optical absorption, compared to high energy transitions present in other TMDs, such as the C peak in MoS_2, where the oscillatory maximum is found.[28] This may partially contribute to the stronger coherent response, as the transient signal is proportional to the first derivative of the absorption. In addition, by calculating the orbital character of the projected (PDOS) band structure, we find that the portion of the conduction band related to the A′ and B′ transitions is strongly hybridized with Te orbitals (up to ∼40%), while at the *K*-point, it is mostly Mo (see Figure S6 in the Supporting Information). Since the A_{1g} vibration involves the out-of-plane motion of Te atoms around the fixed Mo atom, the strongly hybridized regions of band structure are most sensitive to the change in the interatomic distance, i.e., variation in Mo−Te orbital proximity, resulting in a significant energy renormalization. Hence, this explains the extremely intense coherent oscillations observed in 2*H*-$MoTe_2$ as the result of a modulation of the optical absorption due to the out-of-plane atomic displacement launched by the optical pulse.

In conclusion, we investigated the generation and detection of coherent phonons in monolayer 2*H*-$MoTe_2$ using a combination of femtosecond pump−probe microscopy and ab initio calculations. In excellent agreement between experiment and theory, we found that photoexcitation stimulates the out-of-plane A_{1g} vibration, which strongly modulates the absorption in the visible range, especially around the A′ and B′ excitons. We identified a displacive excitation mechanism where photoexcitation shifts the quasi-equilibrium positions of the Te atoms to a larger out-of-plane distance. Our calculations also predict modulations of significant magnitude around the A and B excitons, thus expanding the potential for the coherent control of optical phonons and excitons via optical excitation or applied out-of-plane compressive strain into the NIR region down to ∼1 eV.

https://doi.org/10.1021/acs.nanolett.3c01936
Nano Lett. 2023, 23, 9235−9242

■ ASSOCIATED CONTENT

Supporting Information

The Supporting Information is available free of charge at https://pubs.acs.org/doi/10.1021/acs.nanolett.3c01936.

Details of experimental and computational methods, exciton decay dynamics, damping time including temperature dependence, oscillatory phase analysis, excitation energy dependence, projected band structure calculations (PDF)

■ AUTHOR INFORMATION

Corresponding Author

Giulio Cerullo − *Dipartimento di Fisica, Politecnico di Milano, 20133 Milano, Italy;* orcid.org/0000-0002-9534-2702; Email: giulio.cerullo@polimi.it

Authors

Charles J. Sayers − *Dipartimento di Fisica, Politecnico di Milano, 20133 Milano, Italy*

Armando Genco − *Dipartimento di Fisica, Politecnico di Milano, 20133 Milano, Italy;* orcid.org/0000-0002-1292-2614

Chiara Trovatello − *Dipartimento di Fisica, Politecnico di Milano, 20133 Milano, Italy; Department of Mechanical Engineering, Columbia University, New York, New York 10027, United States;* orcid.org/0000-0002-8150-9743

Stefano Dal Conte − *Dipartimento di Fisica, Politecnico di Milano, 20133 Milano, Italy;* orcid.org/0000-0001-8582-3185

Vladislav O. Khaustov − *Center for Nanotechnology Innovation @ NEST, Istituto Italiano di Tecnologia, 56127 Pisa, Italy; Scuola Normale Superiore, 56127 Pisa, Italy;* orcid.org/0000-0001-6910-5511

Jorge Cervantes-Villanueva − *Institute of Materials Science (ICMUV), University of Valencia, E-46980 Valencia, Spain*

Davide Sangalli − *Division of Ultrafast Processes in Materials (FLASHit), Istituto di Struttura della Materia-CNR (ISM-CNR), 00016 Monterotondo, Scalo, Italy;* orcid.org/0000-0002-4268-9454

Alejandro Molina-Sanchez − *Institute of Materials Science (ICMUV), University of Valencia, E-46980 Valencia, Spain;* orcid.org/0000-0001-5121-4058

Camilla Coletti − *Center for Nanotechnology Innovation @ NEST, Istituto Italiano di Tecnologia, 56127 Pisa, Italy; Graphene Labs, Istituto Italiano di Tecnologia, 16163 Genova, Italy;* orcid.org/0000-0002-8134-7633

Christoph Gadermaier − *Dipartimento di Fisica, Politecnico di Milano, 20133 Milano, Italy;* orcid.org/0000-0001-6613-9644

Complete contact information is available at: https://pubs.acs.org/10.1021/acs.nanolett.3c01936

Author Contributions

C.J.S., C.T., and A.G. performed the experiments with assistance from S.D.C. The experimental data was analyzed by C.J.S. Samples were prepared by V.O.K. with supervision from C.C. Ab initio calculations were performed by J.C.-V. with supervision from D.S. and A.M.-S. The paper was written by C.J.S. and C.G. with input from all authors. G.C. supervised and coordinated the project.

Notes

The authors declare no competing financial interest.

■ ACKNOWLEDGMENTS

This work has received funding from the European Union's Horizon 2020 research and innovation programme under Grant Agreement No. 881603. A.G. acknowledges support by the European Union Marie Sklodowska-Curie Actions (project ENOSIS H2020-MSCA-IF-2020-101029644). C.T. acknowledges the European Union's Horizon Europe Research and Innovation Programme under the Marie Skłodowska-Curie PIONEER HORIZON-MSCA-2021-PF-GF Grant Agreement No. 101066108, and the Optica Foundation and Coherent Inc. for supporting this research through the Bernard J. Couillaud prize. S.D.C. acknowledges financial support from MIUR through the PRIN 2017 program (Prot. 20172H2SC4). A.M.-S. acknowledges the Ramón y Cajal Programme (Grant No. RYC2018-024024-I; MINECO, Spain), Generalitat Valenciana, program SEJIGENT (reference 2021/034), project Magnons in magnetic 2D materials for a novel electronics (2D MAGNONICS), and Planes complementarios de I+D+I en materiales avanzados, project SPINO2D, reference MFA/2022/009. A.M.-S. and J.C.-V. acknowledges the Spanish Ministry of Science MICINN (Project No. PID2020-112507GB-I00, Novel quantum states in heterostructures of 2D materials and Grant No. PRE2021-097581). D.S. acknowledges PRIN BIOX Grant No. 20173B72NB from MIUR (Italy), European Union project MaX Materials design at the eXascale H2020-EINFRA-2015-1 (Grant Agreement No. 824143 & 101093374), and COST Action TUMIEE CA17126, supported by COST (European Cooperation in Science and Technology).

■ REFERENCES

(1) Bardeen, J.; Shockley, W. Deformation Potentials and Mobilities in Non-Polar Crystals. *Phys. Rev.* **1950**, *80*, 72.

(2) Fischetti, M. V.; Laux, S. E. Band Structure, Deformation Potentials, and Carrier Mobility in Strained Si, Ge, and SiGe Alloys. *J. Appl. Phys.* **1996**, *80*, 2234.

(3) Gunst, T.; Markussen, T.; Stokbro, K.; Brandbyge, M. First-principles method for electron-phonon coupling and electron mobility: Applications to two-dimensional materials. *Phys. Rev. B* **2016**, *93*, 035414.

(4) Allen, P. B. Theory of Thermal Relaxation of Electrons in Metals. *Phys. Rev. Lett.* **1987**, *59*, 1460.

(5) Gadermaier, C.; Alexandrov, A. S.; Kabanov, V. V.; Kusar, P.; Mertelj, T.; Yao, X.; Manzoni, C.; Brida, D.; Cerullo, G.; Mihailovic, D. Electron-Phonon Coupling in High-Temperature Cuprate Superconductors Determined from Electron Relaxation Rates. *Phys. Rev. Lett.* **2010**, *105*, 1.

(6) He, X.; Chebl, M.; Yang, D.-S. Cross-Examination of Ultrafast Structural, Interfacial, and Carrier Dynamics of Supported Monolayer MoS_2. *Nano Lett.* **2020**, *20*, 2026−2033.

(7) Molina-Sánchez, A.; Sangalli, D.; Wirtz, L.; Marini, A. Ab initio calculations of ultrashort carrier dynamics in twodimensional materials: Valley depolarization in single-layer WSe_2. *Nano Lett.* **2017**, *17*, 4549.

(8) Selig, M.; Berghauser, G.; Raja, A.; Nagler, P.; Schuller, C.; Heinz, T.; Korn, T.; Chernikov, A.; Malic, E.; Knorr, A. Excitonic Linewidth and Coherence Lifetime in Monolayer Transition Metal Dichalcogenides. *Nat. Comms.* **2016**, *7*, 13279.

(9) Miao, X.; Zhang, G.; Wang, F.; Yan, H.; Ji, M. Layer-Dependent Ultrafast Carrier and Coherent Phonon Dynamics in Black Phosphorus. *Nano Lett.* **2018**, *18*, 3053−3059.

(10) Bartram, M. F.; Leng, Y.-C.; Wang, Y.; Liu, L.; Chen, X.; Peng, H.; Li, H.; Yu, P.; Wu, Y.; Lin, M.-L.; Zhang, J.; Tan, P.-H.; Yang, L. Ultrafast coherent interlayer phonon dynamics in atomically thin layers of MnBi2Te4. *npj Quantum Materials* **2022**, *7*, 84.

(11) Porer, M.; Leierseder, U.; Ménard, J.-M.; Dachraoui, H.; Mouchliadis, L.; Perakis, I. E.; Heinzmann, U.; Demsar, J.; Rossnagel, K.; Huber, R. Non-thermal separation of electronic and structural orders in a persisting charge density wave. *Nat. Mater.* **2014**, *13*, 857.
(12) Hedayat, H.; Sayers, C. J.; Bugini, D.; Dallera, C.; Wolverson, D.; Batten, T.; Karbassi, S.; Friedemann, S.; Cerullo, G.; van Wezel, J.; Clark, S. R.; Carpene, E.; Da Como, E. Excitonic and lattice contributions to the charge density wave in 1*T*-$TiSe_2$ revealed by a phonon bottleneck. *Phys. Rev. Res.* **2019**, *1*, 023029.
(13) Maklar, J.; et al. Nonequilibrium charge-density-wave order beyond the thermal limit. *Nat. Comms.* **2021**, *12*, 2499.
(14) Sayers, C. J.; Dal Conte, S.; Wolverson, D.; Gadermaier, C.; Cerullo, G.; Carpene, E.; Da Como, E. Spectrally Resolving the Phase and Amplitude of Coherent Phonons in the Charge Density Wave State of 1*T*-$TaSe_2$. *Adv. Optical Mater.* **2022**, *10*, 62.
(15) Cerullo, G.; Manzoni, C. Time-Domain Vibrational Spectroscopy: Principle and Experimental Tools. In *Coherent Vibrational Dynamics*; CRC Press: Boca Raton, FL, 2007; Chapter 1, pp 1−48.
(16) Dekorsy, T.; Cho, G. C.; Kurz, H. *Light Scattering in Solids VIII*; Springer, Berlin, Heidelberg, 2010; pp 169−209.
(17) Ishioka, K.; Misochko, O. V. Coherent Lattice Oscillations in Solids and Their Optical Control. In *Progress in Ultrafast Intense Laser Science*, Vol. *98*; Springer, 2010; pp 47−63.
(18) Wang, Q.; Schoenlein, R. W.; Peteanu, L. A.; Mathies, R. A.; Shank, C. V. Vibrationally Coherent Photochemistry in the Femtosecond Primary Event of Vision. *Science* **1994**, *266*, 422−424.
(19) Feldmann, J.; Leo, K.; Shah, J.; Miller, D. A. B.; Cunningham, J. E.; Meier, T.; von Plessen, G.; Schulze, A.; Thomas, P.; Schmitt-Rink, C. Optical Investigation of Bloch oscillations in a semiconductor superlattice. *Phys. Rev. B* **1992**, *46*, 7252−7255.
(20) Dekorsy, T.; Auer, H.; Waschke, C.; Bakker, H. J.; Roskos, H. G.; Kurz, H.; Wagner, V.; Grosse, P. Emission of Submillimeter Electromagnetic Waves by Coherent Phonons. *Phys. Rev. Lett.* **1995**, *74*, 738−741.
(21) Li, J. J.; Zhu, K. D. All-Optical Mass Sensing with Coupled Mechanical Resonator Systems. *Phys. Rep.* **2013**, *525*, 223.
(22) Lanzillotti-Kimura, N. D.; O'Brien, K. P.; Rho, J.; Suchowski, H.; Yin, X.; Zhang, X. Polarization-Controlled Coherent Phonon Generation in Acoustoplasmonic Metasurfaces. *Phys. Rev. B* **2018**, *97*, 23540.
(23) Baldini, E.; Palmieri, T.; Dominguez, A.; Ruello, P.; Rubio, A.; Chergui, M. Phonon-Driven Selective Modulation of Exciton Oscillator Strengths in Anatase TiO2 Nanoparticles. *Nano Lett.* **2018**, *18*, 5007−5014.
(24) Baldini, E.; Dominguez, A.; Palmieri, T.; Cannelli, O.; Rubio, A.; Ruello, P.; Chergui, M. Exciton Control in a Room Temperature Bulk Semiconductor with Coherent Strain Pulses. *Sci. Adv.* **2019**, *5*, 1.
(25) Hase, M.; Katsuragawa, M.; Constantinescu, A. M.; Petek, H. Coherent Phonon-Induced Optical Modulation in Semiconductors at Terahertz Frequencies. *New J. Phys.* **2013**, *15*, 055018.
(26) Luer, L.; Gadermaier, C.; Crochet, J.; Hertel, T.; Brida, D.; Lanzani, G. Coherent Phonon Dynamics in Semiconducting Carbon Nanotubes: A Quantitative Study of Electron-Phonon Coupling. *Phys. Rev. Lett.* **2009**, *102*, 1.
(27) Ni, L. M.; Huynh, U.; Cheminal, A.; Thomas, T. H.; Shivanna, R.; Hinrichsen, T. F.; Ahmad, S.; Sadhanala, A.; Rao, A. Real-Time Observation of Exciton-Phonon Coupling Dynamics in Self-Assembled Hybrid Perovskite Quantum Wells. *ACS Nano* **2017**, *11*, 10834−10843.
(28) Trovatello, C.; et al. Strongly coupled coherent phonons in single-layer MoS_2. *ACS Nano* **2020**, *14*, 5700.
(29) Mor, S.; Gosetti, V.; Molina-Sanchez, A.; Sangalli, D.; Achilli, S.; Agekyan, V. F.; Franceschini, P.; Giannetti, C.; Sangaletti, L.; Pagliara, S. Photoinduced modulation of the excitonic resonance via coupling with coherent phonons in a layered semiconductor. *Phys. Rev. Research* **2021**, *3*, 043175.
(30) Radisavljevic, B.; Radenovic, A.; Brivio, J.; Giacometti, V.; Kis, A. Single-Layer MoS_2 Transistors. *Nat. Nanotechnology* **2011**, *6*, 147.
(31) Wang, Q. H.; Kalantar-Zadeh, K.; Kis, A.; Coleman, J. N.; Strano, M. S. Electronics and Optoelectronics of Two-Dimensional Transition Metal Dichalcogenides. *Nat. Nanotechnology* **2012**, *7*, 699.
(32) Fiori, G.; Bonaccorso, F.; Iannaccone, G.; Palacios, T.; Neumaier, D.; Seabaugh, A.; Banerjee, S. K.; Colombo, L. Electronics Based on Two-Dimensional Materials. *Nat. Nanotechnology* **2014**, *9*, 768.
(33) Jariwala, D.; Sangwan, V. K.; Lauhon, L. J.; Marks, T. J.; Hersam, M. C. Emerging Device Applications for Semiconducting TwoDimensional Transition Metal Dichalcogenides. *ACS Nano* **2014**, *8*, 1102.
(34) Mak, K. F.; Shan, J. Photonics and Optoelectronics of 2D Semiconductor Transition Metal Dichalcogenides. *Nat. Photonics* **2016**, *10*, 216.
(35) Koppens, F. L. H.; Mueller, T.; Avouris, P.; Ferrari, A. C.; Vitiello, M. S.; Polini, M. Photodetectors based on graphene, other two-dimensional materials and hybrid systems. *Nat. Nanotechnology* **2014**, *9*, 780.
(36) Jeong, T. Y.; Jin, B. M.; Rhim, S. H.; Debbichi, L.; Park, J.; Jang, Y. D.; Lee, H. R.; Chae, D.-H.; Lee, D.; Kim, Y.-H.; Jung, S.; Yee, K. J. Coherent Lattice Vibrations in Mono- and Few-Layer WSe_2. *ACS Nano* **2016**, *10*, 5560.
(37) Cho, S.; Kim, S.; Kim, J. H.; Zhao, J.; Seok, J.; Keum, D. H.; Baik, J.; Choe, D. H.; Chang, K. J.; Suenaga, K.; Kim, S. W.; Lee, Y. H.; Yang, H. Phase Patterning for Ohmic Homojunction Contact in $MoTe_2$. *Science* **2015**, *349* (625), 625.
(38) Keum, D. H.; Cho, S.; Kim, J. H.; Choe, D. H.; Sung, H. J.; Kan, M.; Kang, H.; Hwang, J. Y.; Kim, S. W.; Yang, H.; Chang, K. J.; Lee, Y. H. Bandgap Opening in Few-Layered Monoclinic $MoTe_2$. *Nat. Phys.* **2015**, *11*, 482.
(39) Lee, S.; Jang, J.; Kim, S. I.; Jung, S. G.; Kim, J.; Cho, S.; Kim, S. W.; Rhee, J. Y.; Park, K. S.; Park, T. Origin of Extremely Large Magnetoresistance in the Candidate Type-II Weyl Semimetal $MoTe_{2-x}$. *Sci. Rep.* **2018**, *8*, 13937.
(40) Jindal, A.; Saha, A.; Li, Z.; Taniguchi, T.; Watanabe, K.; Hone, J. C.; Birol, T.; Fernandes, R. M.; Dean, C. R.; Pasupathy, A. N.; Rhodes, D. A. Coupled ferroelectricity and superconductivity in bilayer T_d-$MoTe_2$. *Nature* **2023**, *613*, 48−52.
(41) Qi, Y.; et al. Superconductivity in Weyl Semimetal Candidate $MoTe_2$. *Nat. Comms.* **2016**, *7*, 11038.
(42) Ruppert, C.; Aslan, O. B.; Heinz, T. F. Optical Properties and Band Gap of Single- and Few-Layer $MoTe_2$ Crystals. *Nano Lett.* **2014**, *14*, 6231−6236.
(43) Lezama, I. G.; Arora, A.; Ubaldini, A.; Barreteau, C.; Giannini, E.; Potemski, M.; Morpurgo, A. F. Indirect-to-Direct Band Gap Crossover in Few-Layer $MoTe_2$. *Nano Lett.* **2015**, *15*, 2336−2342.
(44) Mleczko, M. J.; Yu, A. C.; Smyth, C. M.; Chen, V.; Shin, Y. C.; Chatterjee, S.; Tsai, Y. C.; Nishi, Y.; Wallace, R. M.; Pop, E. Contact Engineering High-Performance n-Type $MoTe_2$ Transistors. *Nano Lett.* **2019**, *19*, 6352−6362.
(45) Pradhan, N. R.; Rhodes, D.; Feng, S.; Xin, Y.; Memaran, S.; Moon, B. H.; Terrones, H.; Terrones, M.; Balicas, L. Field-Effect Transistors Based on Few-Layered α-$MoTe_2$. *ACS Nano* **2014**, *8*, 5911−5920.
(46) Li, N.; Zhang, J.; Xue, Y.; Zhou, T.; Yang, Z. Large Valley Polarization in Monolayer $MoTe_2$ on a Magnetic Substrate. *Phys. Chem. Chem. Phys.* **2018**, *20*, 3805−3812.
(47) Lin, Y. F.; Xu, Y.; Wang, S. T.; Li, S. L.; Yamamoto, M.; Aparecido-Ferreira, A.; Li, W.; Sun, H.; Nakaharai, S.; Jian, W.; Ueno, B.; Tsukagoshi, K.; Transistors, K. A. M. Logic Circuits, T. A. Ambipolar $MoTe_2$ Transistors and Their Applications in Logic Circuits. *Adv. Mater.* **2014**, *26*, 3263−3269.
(48) Pace, S.; Martini, L.; Convertino, D.; Keum, D. H.; Forti, S.; Pezzini, S.; Fabbri, F.; Miseikis, V.; Coletti, C. Synthesis of Large-Scale Monolayer 1T'-$MoTe_2$ and Its Stabilization via Scalable hBN Encapsulation. *ACS Nano* **2021**, *15*, 4213−4225.
(49) Chi, Z.; Chen, H.; Zhao, Q.; Weng, Y.-X. Ultrafast carrier and phonon dynamics in few-layer 2H−$MoTe_2$. *J. Chem. Phys.* **2019**, *151*, 11470.

https://doi.org/10.1021/acs.nanolett.3c01936
Nano Lett. 2023, 23, 9235−9242

(50) Perlangeli, M.; Peli, S.; Soranzio, D.; Puntel, D.; Parmigiani, F.; Cilento, F. Polarization-resolved broadband time-resolved optical spectroscopy for complex materials: application to the case of $MoTe_2$ polytypes. *Opt. Exp.* **2020**, *28*, 8819.
(51) Schulzetenberg, A.; Johns, J. Chemical defects control the exciton lifetime in CVD grown, few-layer $MoTe_2$. *Electron. Struct.* **2021**, *3*, 025001.
(52) Attar, A. R.; Chang, H.-T.; Britz, A.; Zhang, X.; Lin, M.-F.; Krishnamoorthy, A.; Linker, T.; Fritz, D.; Neumark, D. M.; Kalia, R. K.; Nakano, A.; Ajayan, P.; Vashishta, P.; Bergmann, U.; Leone, S. R. Simultaneous Observation of Carrier-Specific Redistribution and Coherent Lattice Dynamics in 2H-$MoTe_2$ with Femtosecond Core-Level Spectroscopy. *ACS Nano* **2020**, *14*, 15829.
(53) Wang, Z.; Altmann, P.; Gadermaier, C.; Yang, Y.; Li, W.; Ghirardini, L.; Trovatello, C.; Finazzi, M.; Duò, L.; Celebrano, M.; Long, R.; Akinwande, D.; Prezhdo, O. V.; Cerullo, G.; Dal Conte, S. Phonon-Mediated Interlayer Charge Separation and Recombination in a $MoSe_2/WSe_2$ Heterostructure. *Nano Lett.* **2021**, *21*, 2165−2173.
(54) Froehlicher, G.; Lorchat, E.; Fernique, F.; Joshi, C.; Molina-Sánchez, A.; Wirtz, L.; Berciaud, S. Unified Description of the Optical Phonon Modes in N-Layer $MoTe_2$. *Nano Lett.* **2015**, *15*, 6481.
(55) Wilson, J. A.; Yoffe, A. D. The transition metal dichalcogenides discussion and interpretation of the observed optical, electrical and structural properties. *Adv. Phys.* **1969**, *18*, 193−335.
(56) Pogna, E. A. A.; Marsili, M.; De Fazio, D.; Dal Conte, S.; Manzoni, C.; Sangalli, D.; Yoon, D.; Lombardo, A.; Ferrari, A. C.; Marini, A.; Cerullo, G.; Prezzi, D. Photo-Induced Bandgap Renormalization Governs the Ultrafast Response of Single-Layer MoS_2. *ACS Nano* **2016**, *10*, 1182−1188.
(57) Trovatello, C.; Katsch, F.; Li, Q.; Zhu, X.; Knorr, A.; Cerullo, G.; Dal Conte, S. Disentangling Many-Body Effects in the Coherent Optical Response of 2D Semiconductors. *Nano Lett.* **2022**, *22*, 5322−5329.
(58) Li, T.; Zhang, Z.; Zheng, W.; Lv, Y.; Huang, F. A possible high-mobility signal in bulk $MoTe_2$: Temperature independent weak phonon decay. *AIP Advances* **2016**, *6*, 115207.
(59) Dhar, L.; Rogers, J. A.; Nelson, K. A. Time-Resolved Vibrational Spectroscopy in the Impulsive Limit. *Chem. Rev.* **1994**, *94*, 157−193.
(60) Zeiger, H. J.; Vidal, J.; Cheng, T. K.; Ippen, E. P.; Dresselhaus, G.; Dresselhaus, M. S. Theory for Displacive Excitation of Coherent Phonons. *Phys. Rev. B* **1992**, *45*, 768−778.
(61) Molina-Sánchez, A.; Catarina, G.; Sangalli, D.; Fernández-Rossier, J. Magneto-optical response of chromium trihalide monolayers: chemical trends. *J. Mater. Chem. C* **2020**, *8*, 8856−8863.
(62) Bernardi, M.; Palummo, M.; Grossman, J. C. Extraordinary Sunlight Absorption and One Nanometer Thick Photovoltaics Using Two-Dimensional Monolayer Materials. *Nano Lett.* **2013**, *13*, 3664−3670.

https://doi.org/10.1021/acs.nanolett.3c01936
Nano Lett. 2023, 23, 9235−9242